

# Melting-solidification transition of Zn nanoparticles embedded in SiO<sub>2</sub>: Observation by synchrotron x-ray and ultraviolet-visible-near-infrared light

H. Amekura (雨倉宏),<sup>1,a)</sup> M. Tanaka (田中雅彦),<sup>2</sup> Y. Katsuya (勝矢良雄),<sup>3</sup>  
H. Yoshikawa (吉川英樹),<sup>2</sup> M. Ohnuma (大沼正人),<sup>4</sup> Y. Matsushita (松下能孝),<sup>2</sup>  
K. Kobayashi (小林啓介),<sup>2</sup> and N. Kishimoto (岸本直樹)<sup>1</sup>

<sup>1</sup>*Ion Beam Group, National Institute for Materials Science (NIMS), 3-13 Sakura, Tsukuba, Ibaraki 305-0003, Japan*

<sup>2</sup>*NIMS Beamline Station at SPring-8, National Institute for Materials Science (NIMS),*

*1-1-1 Kouto, Sayo-cho, Hyogo 679-5148, Japan*

<sup>3</sup>*SPring-8 Service Co. Ltd., 1-1-1 Kouto, Sayo-cho, Hyogo 679-5148, Japan*

<sup>4</sup>*Neutron Scattering Group, National Institute for Materials Science (NIMS), 1-2-1 Sengen, Tsukuba, Ibaraki 305-0047, Japan*

(Received 16 June 2010; accepted 28 August 2010; published online 17 November 2010)

Melting-solidification transition of Zn nanoparticles (NPs) with the mean diameter of 11.5 nm, embedded in silica glass, was investigated by glancing incident x-ray diffraction (GIXRD) at high temperatures using synchrotron radiation (SR). With increasing temperature, 101<sub>Zn</sub> diffraction peak gradually decreases up to ~360 °C and then steeply decreases. This is due to the melting of Zn NPs, which completes around 420 °C. With decreasing temperature, the solidification of the NPs begins around ~310 °C. The temperature hysteresis with a width of ~110 °C was observed. With temperature, the diffraction angle shows a shift without hysteresis, which is ascribed to thermal expansion of Zn NP lattice. Thermal expansion coefficient of Zn NPs was determined as  $24.4 \times 10^{-6} \text{ K}^{-1}$  along the  $\langle 101 \rangle$  direction. Optical absorption spectroscopy shows a broad ultraviolet (UV) peak which was observed at even higher temperatures than the melting temperature but shifts to the low-energy side with the melting. The energy shift in the UV peak also shows the temperature hysteresis which resembles with the melting-solidification hysteresis recorded by SR-GIXRD. The melting-solidification transition is also detectable by the optical absorption spectroscopy in the UV-visible-near-infrared region. © 2010 American Institute of Physics. [doi:10.1063/1.3494098]

## I. INTRODUCTION

The solid-liquid (SL) transition is one of the phase transitions known since ancient times, and the SL transitions of nanophases still fascinate many scientists<sup>1-12</sup> because they are different from those of their bulk counterparts in terms of both the transition temperatures<sup>1-3</sup> and transition modes.<sup>4-6</sup> For example, while the melting point ( $T_{\text{mp}}$ ) of bulk gold is 1064.4 °C, that of gold nanoparticles (NPs) on substrate decreases to 830 °C as the particle diameter decreases to 5 nm;<sup>2</sup> i.e.,  $\Delta T_{\text{mp}} = T_{\text{mp}}^{\text{NPs}} - T_{\text{mp}}^{\text{bulk}} \sim -230 \text{ °C}$ . The  $T_{\text{mp}}$  of NPs embedded in a solid matrix is more difficult to predict, because not only the size but also the pressure from the matrix influences the  $T_{\text{mp}}$ . In fact, xenon NPs embedded in aluminum maintain a crystalline state even at room temperature (RT), although the  $T_{\text{mp}}$  of bulk Xe under atmospheric pressure is -111.9 °C; i.e.,  $\Delta T_{\text{mp}} > +140 \text{ °C}$ .<sup>3</sup> Since both of these effects contribute to  $T_{\text{mp}}$  in different ways, experimental determination of  $T_{\text{mp}}$  is essential for embedded NPs.

For several years, we have proposed thermal oxidation of Zn NPs embedded in SiO<sub>2</sub>, which were previously fabricated by ion implantation, as a successful route for fabricating ZnO NPs of high quality.<sup>13,14</sup> While a temperature of 700 °C is required for efficient oxidation of Zn NPs to ZnO NPs, the question arises as to whether the embedded Zn NPs

are in a crystalline or a liquid phase during oxidation at that temperature. One of the objectives of this study is to clarify this point.

Up to now, the melting behaviors of embedded NPs have been evaluated by various methods including transmission electron microscopy,<sup>3,7-9</sup> x-ray diffraction (XRD),<sup>8,9</sup> and Rutherford backscattering spectrometry.<sup>9</sup> A search of the literature found only two reports describing optical absorption studies on the melting of Au NPs (Ref. 10) and Cu NPs (Ref. 11) in silica glass (SiO<sub>2</sub>), in which they ascribed some changes in optical absorption to the melting behaviors. While these authors ascribed several changes in the optical absorption to the surface melting and to bulk melting of NPs, etc, the results are not free from criticism because they did not determine  $T_{\text{mp}}$  experimentally but presumed the  $T_{\text{mp}}$  value from data in the literature while disregarding the large uncertainty of  $T_{\text{mp}}$  in the case of embedded NPs.

In this paper, we describe a study in which we experimentally determined the melting and solidification behaviors of Zn NPs embedded in SiO<sub>2</sub> at high temperatures (HTs) by the glancing incident XRD (GIXRD) using synchrotron radiation (SR). However, if the size of the NPs might change during the HT measurements, it caused serious difficulty in interpretation of the results. Little change in size of the NPs during the HT measurements was experimentally confirmed by small-angle x-ray scattering (SAXS). In addition to the melting-solidification transition, thermal expansion behavior

<sup>a)</sup>Electronic mail: amekura.hiroshi@nims.go.jp.

of Zn NPs is determined from the temperature dependence of the diffraction angle. Furthermore, changes in the optical absorption spectrum of Zn NPs in the ultraviolet (UV) to the near-infrared (NIR) regions induced by the melting and solidification were studied. Optical detection of the melting-solidification transitions is also shown.

In the previous letter,<sup>15</sup> we described effects of melting of Zn NPs on the surface plasmon resonances (SPRs). The main topic was the SPRs, and the SL transition was used to change the parameters which influenced the SPRs. In this paper, the main topic is rather the SL transition of Zn NPs. In the latter half of this paper, the changes in the optical absorption was used to observe the SL transition.

## II. EXPERIMENTAL

Zn NPs were formed in SiO<sub>2</sub> substrate of the KU-1 type (OH ~ 820 ppm) by implantation of Zn ions of 60 keV up to a fluence of  $1.0 \times 10^{17}$  ions/cm<sup>2</sup>. The formation parameters were the same as those reported in our previous studies.<sup>13,14,16,17</sup> Since Zn NPs are formed in the surface layer of 70–80 nm thick only, we applied a method sensitive to the surface layer, i.e., the GIXRD, to monitor the SL transition of the Zn NPs. However, because an excessively long measurement duration at HTs might cause coarsening of the NPs, we used a high-intensity x-ray from a SR facility to shorten the measurement duration. A HT sample holder was installed in the vacuum chamber of the high-resolution diffractometer<sup>18</sup> of the BL15XU beamline at the SPring-8 SR facility, Japan. The sample was kept in a vacuum to avoid oxidation during the HT measurements. Three sets of thermocouples were used: one was installed in the sample holder to apply the PID control, and the others were attached to the surface side and to the rear side, respectively, of the sample. The thermocouple of the surface side was covered by another glass to avoid the direct irradiation of the x-ray, whose value was assumed as the temperature of the NPs. We estimate that the relative temperature has uncertainty of 1 °C, while the absolute value of the temperature includes uncertainty of ~20 °C. An x-ray energy of 5.415 keV was used, which corresponds to the chromium  $K_{\alpha 1}$  line. Diffraction patterns were recorded by a yttrium aluminum perovskite (YAP) scintillator detector through 10 cm soller slits with scanning a scattering angle of  $2\theta$ , where the incident angle  $\theta_{inc}$  was fixed at 3°.

Before the measurements were initiated, the sample was heated once to 500 °C in a vacuum. This procedure prevented coarsening during the HT measurements, so that if coarsening occurred it would be induced before the measurements. Moreover, the size distributions of the NPs were evaluated before and after the HT measurements by SAXS. The details of the SAXS measurements are described elsewhere.<sup>16</sup>

HT measurements might induce oxidation of Zn NPs with residual oxygen in the chamber then the formation of ZnO phase, or further reaction of ZnO phase with SiO<sub>2</sub> substrate then the formation of Zn<sub>2</sub>SiO<sub>4</sub> phase. In fact, the same starting material, i.e., Zn NPs in SiO<sub>2</sub>, is transformed to ZnO and Zn<sub>2</sub>SiO<sub>4</sub> phases after HT annealing in oxygen ambient at

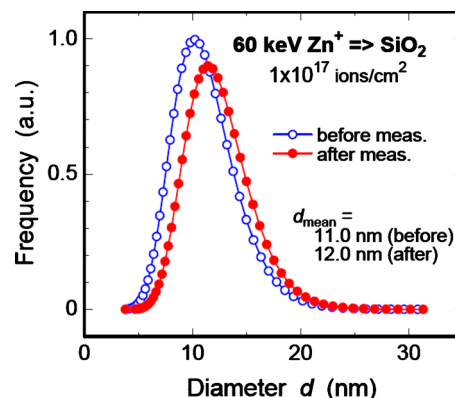


FIG. 1. (Color online) Size distributions of Zn NPs before (line with open circles) and after (line with closed circles) high-temperature GIXRD measurements, determined by lab-SAXS measurements. The experimental details are described in Ref. 16.

700 °C and 900 °C, respectively.<sup>14,17</sup> These reference samples were formed and evaluated by laboratory GIXRD apparatus with a position-sensitive proportional counter. The same incident angle of 3° and x-ray energy of 5.415 keV were used.

In addition to the HT-GIXRD measurements in the SR facility, optical transmission spectroscopy was carried out at HTs using a conventional double-beam UV-visible-NIR spectrometer equipped with another HT vacuum sample chamber. The wavelength region and the resolution were 215–1700 nm and 2 nm, respectively.

## III. RESULTS AND DISCUSSION

### A. Synchrotron XRD

Figure 1 shows the size distributions of Zn NPs before and after the GIXRD measurements at HTs, which were determined by the SAXS measurements. The mean diameter was, respectively, 11.0 nm and 12.0 nm before and after the measurements, indicating that coarsening of the NPs during the measurements is small and can be considered negligible. The negligible size changes simplify the interpretation of data shown in this paper.

Figure 2 shows SR-GIXRD patterns from Zn NPs at various temperatures recorded in rising temperature sequence. As shown later, the results depend on the temperature sequence, rising or falling, because the melting-solidification transition shows a hysteresis due to a nature of the first order phase transition.

At 74 °C, Zn NPs show a strong peak of 101<sub>Zn</sub> diffraction around  $2\theta=66.2^\circ$ , and less clear peaks of 100<sub>Zn</sub> and 002<sub>Zn</sub> around  $55.1^\circ$  and  $59.4^\circ$ , respectively. With increasing  $T$ , the 101<sub>Zn</sub> peak gradually decreases and shifts to the low  $2\theta$  side, up to ~385 °C. Above ~385 °C, the peak steeply decreases. The peaks of 100<sub>Zn</sub> and 002<sub>Zn</sub> also gradually decrease up to 385 °C but disappear above 385 °C.

Patterns from intentionally oxidized (ZnO NPs) and intentionally reacted with SiO<sub>2</sub> matrix (Zn<sub>2</sub>SiO<sub>4</sub>) are also shown in Fig. 2, which were measured using lab-GIXRD. Whole the HT experiments of Zn NPs, peaks which could be

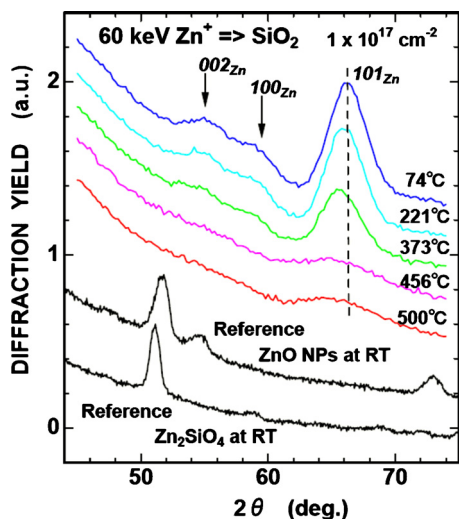


FIG. 2. (Color online) Diffraction patterns from Zn NPs embedded in  $\text{SiO}_2$  detected at various temperatures in a rising  $T$  sequence. For reference, diffraction patterns from ZnO NPs (Ref. 13) and from  $\text{Zn}_2\text{SiO}_4$  nanofilm (Ref. 17) are shown in the lower part.

ascribed to ZnO or  $\text{Zn}_2\text{SiO}_4$  were not observed, excluding possible oxidation and reaction of Zn NPs to other compounds.

Figure 3 shows detailed temperature dependence of the  $101_{\text{Zn}}$  diffraction peak detected in (a) the rising  $T$  and (b) falling  $T$  sequences, respectively. Different behaviors were observed between the rising- and falling- $T$  sequences: for example, the pattern at  $368^\circ\text{C}$  in the rising sequence clearly show the diffraction peak of the crystalline Zn NPs, while the pattern at the same temperature in the falling sequence shows a very weak and broad peak which is ascribed to molten Zn NPs.

Temperature dependences of the peak height and of the full width at half maximum (FWHM) of the  $101_{\text{Zn}}$  diffraction peak are plotted in Figs. 4(a) and 4(b), respectively. The upward and downward triangles show data points recorded

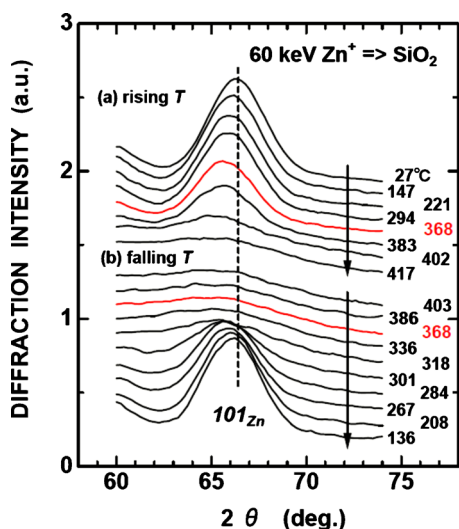


FIG. 3. (Color online) Detailed temperature dependence of diffraction patterns of  $101_{\text{Zn}}$  peak from Zn NPs embedded in  $\text{SiO}_2$ , recorded in (a) rising and (b) falling  $T$  sequences. See the diffraction patterns recorded at the same temperature  $368^\circ\text{C}$  in the rising and falling  $T$  sequences.

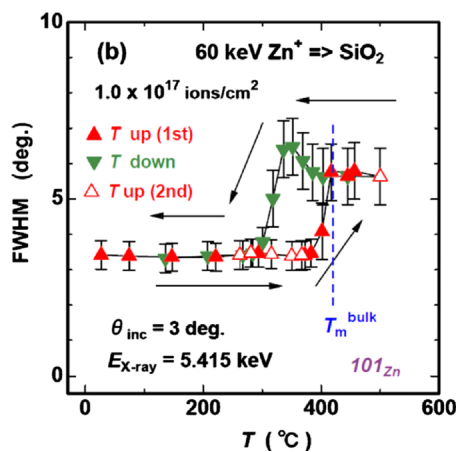
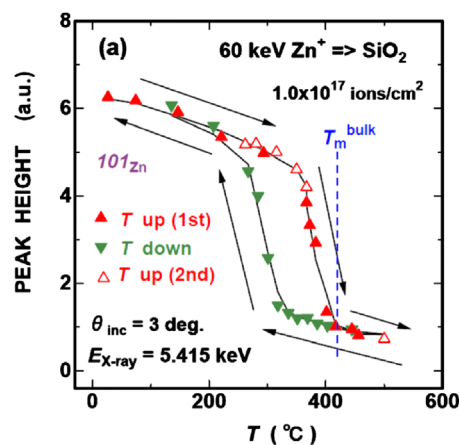


FIG. 4. (Color online) Temperature dependences of (a) the peak height and of (b) the FWHM of  $101_{\text{Zn}}$  diffraction from Zn NPs embedded in  $\text{SiO}_2$  detected by SR-GIXRD. The upward and downward triangles show data points taken in the rising- and falling-temperature sequences, respectively. The closed and open upward triangles show data taken in the first and second runs, respectively. The solid lines are guides for the eye. The dashed line indicates the melting point of bulk Zn.

in the rising- and falling- $T$  sequences, respectively. With increasing temperature, the peak height shows a gradual decrease until  $\sim 360^\circ\text{C}$  and then steeply decreases. Contrary, the width keeps the constant value up to  $\sim 360^\circ\text{C}$  and then steeply increases. The temperature-independent width can be due to a bad resolution of the measurement system, because we aimed to measure the diffraction peaks as quick as possible. The steep decrease in the peak height and the increase in the peak width complete at around  $420^\circ\text{C}$ , which is very close to the bulk  $T_{\text{mp}}$  of  $419.6^\circ\text{C}$ . The steep decrease in the diffraction intensity and the increase in the FWHM are both ascribed to the melting of Zn NPs.

On the other hand, in the falling- $T$  sequence the peak height maintains a low value which corresponds to the molten phase even when the temperature falls to  $\sim 310^\circ\text{C}$ , then shows a steep increase as the temperature falls further to  $\sim 250^\circ\text{C}$ . The peak width is almost constant within error bars down to  $\sim 310^\circ\text{C}$ , and then steeply decreases. A temperature hysteresis with a width of  $\sim 110^\circ\text{C}$  was observed.

After solidification was completed in the falling sequence, the temperature was increased again (second run). The data for the second run are indicated by open triangles in

TABLE I. The best fitting parameters of temperature dependence of  $d$ -value of the  $101_{\text{Zn}}$  diffraction peak from Zn NPs embedded in  $\text{SiO}_2$ .

$d = d_0 + pT(^{\circ}\text{C})$
$p = 5.09 \times 10^{-5} \text{ \AA}/^{\circ}\text{C}$
$d_0 = 2.09 \text{ \AA}$

the figures. The second-run data show a close correspondence with the curve of the first-run data, confirming that the hysteresis was not due to spurious effects but reproducible.

It should be noted that temperature hysteresis is a relatively common phenomenon in the SL transitions of embedded NPs.<sup>7-9</sup> We consider that this is because each NP is separated from other NPs by a matrix. In the cases of thin film, once stable nucleation, mostly due to heterogeneous origins, occurs at any parts of the film, soon the nucleation propagates to all the parts of the film. Consequently, although the SL transition is the first order phase transition, thin films show relatively narrower hysteresis than those expected from the homogenous phase transition theory, or practically no temperature hysteresis.<sup>8</sup> However, in the cases of NPs embedded in a matrix, once the nucleation occurs in a NP, the nucleation cannot propagate to the other NPs because they are separated by the matrix. When the phase transition of NP system occurs, all the NPs independently each other should induce the nucleation inside each the NP. Consequently relatively wider hysteresis is observed.

As shown in Figs. 2 and 3, the diffraction angle shifts to the low angle side with increasing temperature. The temperature dependence of the diffraction angle is plotted in term of the  $d$ -value which relates with the diffraction angle  $2\theta$  following relationship:

$$d = \frac{\lambda}{2 \sin(2\theta/2)}, \quad (1)$$

where  $\lambda$  denotes the wavelength of the x-ray 2.2896  $\text{\AA}$  and  $2\theta$  is in the unit of radian. The data points fall on a linear function of temperature without hysteresis, which is fitted by

$$d = pT(^{\circ}\text{C}) + d_0, \quad (2)$$

where  $T$  denotes temperature in the unit of  $^{\circ}\text{C}$ ,  $d_0$  the  $d$ -value at  $0^{\circ}\text{C}$ , and  $p$  the proportional constant, respectively. From the least-squared fitting of the data, the values were determined as  $p = 5.09 \times 10^{-5} \text{ \AA}/^{\circ}\text{C}$  and  $d_0 = 2.09 \text{ \AA}$  as summarized in Table I. Thermal expansion coefficient  $\beta$  which is defined as

$$\beta = \frac{1}{L} \frac{dL}{dT}, \quad (3)$$

was determined from these data, where  $L$  denotes a certain length along a direction of interest. The coefficient of Zn NPs along the  $\langle 101 \rangle$  direction,  $\beta_{\text{NP}\langle 101 \rangle}$ , is given as  $\beta_{\text{NP}\langle 101 \rangle} \sim p/d_0 = 24.4 \times 10^{-6} \text{ }^{\circ}\text{C}^{-1}$ . As for bulk Zn, the coefficients are known as  $\beta_{\text{bulk}\langle 001 \rangle} = 64.3 \times 10^{-6} \text{ }^{\circ}\text{C}^{-1}$  and  $\beta_{\text{bulk}\langle 100 \rangle} = 13.0 \times 10^{-6} \text{ }^{\circ}\text{C}^{-1}$  at  $20^{\circ}\text{C}$  (Ref. 19) as summarized in Table II. From elementary geometrical consideration, the coefficient  $\beta_{\text{bulk}\langle 101 \rangle}$  is given as

TABLE II. Thermal expansion coefficient  $\beta$  of Zn NPs embedded in  $\text{SiO}_2$  and those of bulk Zn and of silica glass.

	$\beta = \frac{1}{L} \frac{dL}{dT}$ ( $\text{K}^{-1}$ )	Direction	Reference
Zn NPs embedded in $\text{SiO}_2$ (300–700 K)	$24.4 \times 10^{-6}$	$\langle 101 \rangle$	This work
Bulk Zn (293 K)	$22.2 \times 10^{-6}$	$\langle 101 \rangle$	<sup>a</sup>
	$64.3 \times 10^{-6}$	$\langle 001 \rangle$	19
	$13.0 \times 10^{-6}$	$\langle 100 \rangle$	19
Silica glass (300 K)	$0.35 \times 10^{-6}$	...	19

<sup>a</sup>The value of bulk Zn  $\langle 101 \rangle$  direction was calculated from Eq. (4).

$$\beta_{\text{bulk}\langle 101 \rangle} = \frac{4c^2}{3a^2 + 4c^2} \beta_{\text{bulk}\langle 100 \rangle} + \frac{3a^2}{3a^2 + 4c^2} \beta_{\text{bulk}\langle 001 \rangle}, \quad (4)$$

where  $a$  and  $c$  denote the lattice constants of  $a$ - and  $c$ -axis, respectively. The Eq. (4) gives the coefficient of  $22.2 \times 10^{-6} \text{ }^{\circ}\text{C}^{-1}$ , which is in a good agreement with the value of the NPs. This agreement is rather surprising, because the NPs are embedded in silica glass which has a much smaller value of thermal expansion coefficient of  $0.35 \times 10^{-6} \text{ }^{\circ}\text{C}^{-1}$  at  $27^{\circ}\text{C}$ .<sup>19</sup> We expected reduction in thermal expansion of Zn NPs by silica glass matrix, but this is not the case. Possibly structural relaxation is induced in the glass matrix at such low temperature. Defective structure of the glass matrix introduced by ion implantation may play a certain role. Anyway, the temperature-dependent shift in the diffraction angle is ascribed to the thermal expansion of Zn NP lattice (Fig. 5).

## B. Optical detection of melting-solidification

The optical density spectra detected in the rising  $T$  sequence are shown in Fig. 6. With increasing temperature, the NIR peak at 1.2 eV gradually increases in width and decreases in height. The NIR peak is faintly visible at  $363^{\circ}\text{C}$ , but is no longer visible at  $441^{\circ}\text{C}$ . Since the GIXRD peak steeply decreases between 360 and  $420^{\circ}\text{C}$ , the disappear-

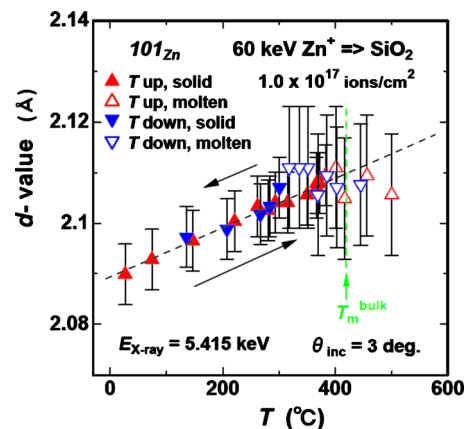


FIG. 5. (Color online) Temperature dependence of  $d$ -value of the  $101_{\text{Zn}}$  diffraction from Zn NPs embedded in  $\text{SiO}_2$ . Upper and lower triangles show data points recorded in the rising and falling  $T$  sequences, respectively. Closed and open triangles correspond to data points in the solid and molten phases, respectively. A broken line indicates the best fitting by Eq. (2).

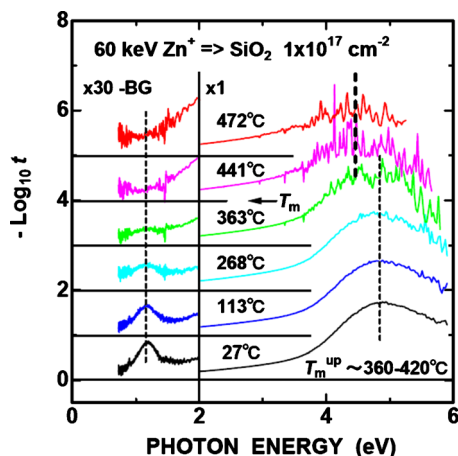


FIG. 6. (Color online) Temperature dependence of the optical density spectra, i.e.,  $-\log_{10} t$ , in the NIR, visible, and UV regions, where  $t$  denotes the optical transmittance. The spectra in the NIR region were magnified 30 times and the backgrounds were subtracted.

ance of the NIR peak can be considered to be coincident with the melting. It is well known that broadening of surface SPR is induced by reduction in the mean-free-path (MFP) of conduction electrons,<sup>20</sup> and the melting steeply reduces the MFP to the order of the lattice constant. On the contrary, the UV peak around 4.8 eV survives even at higher temperatures than 420 °C where the GIXRD data show the melting of all of the Zn NPs. From this different temperature dependence, the NIR and UV peaks are ascribed to different origins. While the assignment of these peaks will be discussed elsewhere,<sup>15</sup> we ascribe the NIR and UV peaks to intraband- and interband-transition enhanced by SPR effect.

While the UV peak energy hardly changes from RT to  $\sim 330$  °C, the peak suddenly shifts to  $\sim 0.3$  eV lower energy with the occurrence of melting. Since the melting is a transition from the crystalline phase to the liquid phase, i.e., similar to the amorphous phase, the energy shift in the optical transition is quite acceptable. In fact, shifts in band-gap energies are reported in some nonmetallic solids with the transition from a crystalline phase to a solid amorphous phase.<sup>21,22</sup> It should be noted that although there are many sharp lines superimposed on the broad UV peak at HTs, they are artifacts because they have no reproducibility in terms of positions and intensities.<sup>23</sup>

To confirm that the shift in the UV peak is due to melting, the temperature dependence of the UV peak was evaluated in both the rising and falling  $T$  sequences. In addition to the sudden shift in the peak energy, the low-energy shoulder of the UV peak also showed a similar sudden shift with melting as shown in Fig. 7. While the peak tail around 3 eV remains almost the same spectral shape and intensity up to 377 °C in the rising  $T$  sequence, it steeply shifts around 400 °C in coincident with the melting as shown in Fig. 7(a). After the melting, the peak tail remains the same spectral shape and intensity even with increasing  $T$  further. (Compare the spectra at 420 and 466 °C). In the falling sequence, the peak tail remains almost the same spectral shape and intensity down to 336 °C and then steeply shifts around 315 °C in coincident with the solidification.

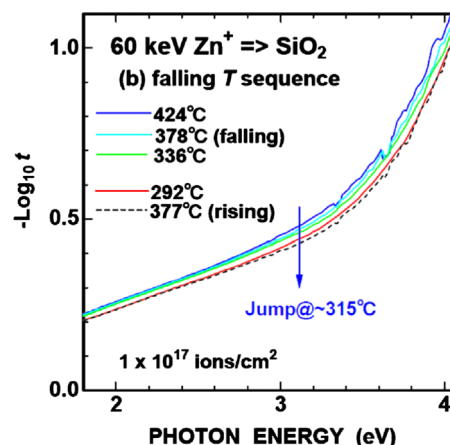
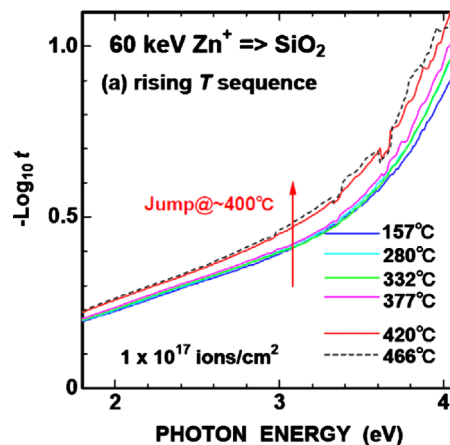


FIG. 7. (Color online) Low-energy tails of optical density spectra, i.e.,  $-\log_{10} t$ , of Zn NPs embedded in  $\text{SiO}_2$  at various temperatures, detected in (a) rising and (b) falling  $T$  sequence.

Since the peak is very broad and very noisy, the determination of the peak energy includes large uncertainty. Instead of the peak energy, the transmittance value at a fixed energy in the tail region of the UV peak, e.g., 3.1 eV, where the S/N ratio is relatively better, can serve a more useful measure of the energy shift. As shown in Fig. 8, the transmittance at 3.1 eV exhibits an almost constant value of  $\sim 38\%$  up to  $\sim 375$  °C in the rising sequence and then steeply decreases at higher temperatures. This is due to the sudden low-energy shift in the UV peak, which is a consequence of the melting of the NPs. In the falling sequence, a low transmittance value is maintained down to  $\sim 335$  °C then the transmittance returns to a high level. Temperature hysteresis is also observed in the optical absorption, which is similar to that observed in the XRD results shown in Fig. 4. The optical detection of the melting-solidification transition is possible for NPs embedded in transparent matrix.

### C. The phase of Zn NPs at 700 °C

Finally, we mention one of the objectives of this study, i.e., the phase of the Zn NPs at 700 °C. Because of a limit of the apparatus used we could not raise the sample temperature up to 700 °C. However, as shown in Figs. 4(a) and 4(b), we have confirmed that the Zn NPs melt at 420 °C or lower

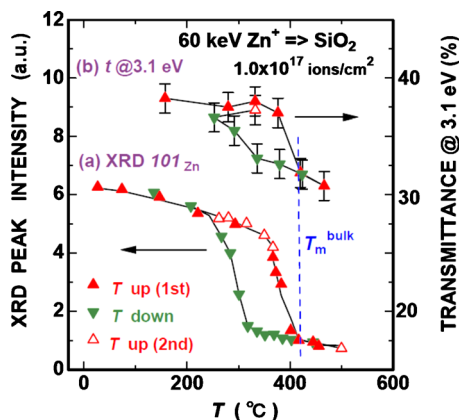


FIG. 8. (Color online) Temperature dependence of (a) the optical transmittance  $t$  detected at a fixed photon energy of 3.1 eV and of (b) the peak intensity of  $101_{\text{Zn}}$  diffraction from Zn NPs embedded in  $\text{SiO}_2$  detected by SR-GIXRD. The upward and downward triangles show data points taken in the rising- and falling-temperature sequences, respectively. The closed and open upward triangles show data taken in the first and second runs, respectively. The solid lines are guides for the eye. The dashed line indicates the melting point of bulk Zn.

temperatures and keep the molten phase at least up to 500 °C. It is expected that they are also in the molten phase around 700 °C, where efficient oxidation to ZnO NPs occurs.<sup>13,14</sup> It should be noted that the boiling temperature of bulk Zn is 907 °C. Since the melting temperatures of Zn NPs do not largely deviate from the bulk value, the boiling temperatures of Zn NPs are estimated much higher than 700 °C.

#### IV. CONCLUSIONS

Several years ago, we have proposed a formation process of ZnO NPs in good quality, using Zn-ion implantation to  $\text{SiO}_2$  and thermal oxidation.<sup>13,14</sup> While a temperature of 700 °C is required for efficient oxidation from Zn NPs to ZnO NPs, the question arises as to whether the embedded Zn NPs are in a crystalline or a liquid phase during oxidation at that temperature. Melting-solidification transition of Zn NPs embedded in  $\text{SiO}_2$ , which were fabricated by Zn-ion implantation, was investigated by SR-GIXRD. With increasing temperature, the  $101_{\text{Zn}}$  diffraction peak from the NPs gradually decreases up to  $\sim 360$  °C, and then steeply decreases. This is due to the melting of Zn NPs and the melting completes around 420 °C. The solidification of the NPs begins around  $\sim 310$  °C. A temperature hysteresis with a width of  $\sim 110$  °C in was observed. Before and after the whole measurements, size distribution of NPs was evaluated by SAXS, in order to exclude thermal coarsening of the NPs during the measurements.

With increasing temperature, the diffraction angle of the  $101_{\text{Zn}}$  peak shifts to the low  $2\theta$  side due to thermal expansion of the NP lattice. Thermal expansion coefficient of Zn NPs was determined as  $24.4 \times 10^{-6} \text{ } ^\circ\text{C}^{-1}$  along the  $\langle 101 \rangle$  direction, which is in a good agreement with the bulk value while the NPs are embedded in silica glass whose thermal expansion coefficient is two orders smaller.

Optical absorption spectroscopy shows that the broad UV peak is observed at even higher than the melting tem-

perature but shifts to the low-energy side with the melting. The energy shift in the UV peak also shows the temperature hysteresis which resembles with the hysteresis obtained by SR-GIXRD measurements. The melting-solidification transition of NPs embedded in transparent matrix can be also detectable by the optical absorption spectroscopy.

It has been estimated from this study that the embedded Zn NPs are in molten phase during thermal oxidation at 700 °C; i.e., the ZnO NPs are formed by thermal oxidation of molten Zn NPs embedded in silica glass.

#### ACKNOWLEDGMENTS

The authors thank the staffs of BL15XU, NIMS and of SPring-8 for their help at the beamline. The GIXRD measurements at HT were performed under the approval of NIMS Beamline Station (Proposal No. 2006B4501, 2007A4501, and 2007B4502). The authors also thank Mr. C. Scholtysik and Professor S. Mantl (FZ Juelich) for Zn-ion implantation.

- <sup>1</sup>M. Takagi, *J. Phys. Soc. Jpn.* **9**, 359 (1954).
- <sup>2</sup>P. Buffat and J.-P. Borel, *Phys. Rev. A* **13**, 2287 (1976).
- <sup>3</sup>S. E. Donnelly, R. C. Birtcher, C. W. Allen, I. Morrison, K. Furuya, M. Song, K. Mitsuishi, and U. Dahmen, *Science* **296**, 507 (2002).
- <sup>4</sup>W. Krakow, M. José-Yacamán, and J. L. Aragón, *Phys. Rev. B* **49**, 10591 (1994).
- <sup>5</sup>J. Harada and K. Ohshima, *Surf. Sci.* **106**, 51 (1981).
- <sup>6</sup>Y. Oshima and K. Takayanagi, *Z. Phys. D: At., Mol. Clusters* **27**, 287 (1993).
- <sup>7</sup>Q. Xu, I. D. Sharp, C. W. Yuan, D. O. Yi, C. Y. Liao, A. M. Glaeser, A. M. Minor, J. W. Beeman, M. C. Ridgway, P. Kluth, J. W. Ager III, D. C. Chrzan, and E. E. Haller, *Phys. Rev. Lett.* **97**, 155701 (2006).
- <sup>8</sup>M. A. Taglienti, G. Mattei, L. Tapfer, M. V. Antisari, and P. Mazzoldi, *Phys. Rev. B* **70**, 075418 (2004).
- <sup>9</sup>H. H. Andersen and E. Johnson, *Nucl. Instrum. Methods Phys. Res. B* **106**, 480 (1995).
- <sup>10</sup>D. Dalacu and L. Martinu, *Appl. Phys. Lett.* **77**, 4283 (2000).
- <sup>11</sup>O. A. Yeshchenko, I. M. Dmitruk, A. A. Alexeenko, and A. M. Dmytruk, *Phys. Rev. B* **75**, 085434 (2007).
- <sup>12</sup>J. A. Pakarinen, M. Backman, F. Djurabekova, and K. Nordlund, *Phys. Rev. B* **79**, 085426 (2009).
- <sup>13</sup>H. Amekura, N. Umeda, Y. Sakuma, N. Kishimoto, and C. Buchal, *Appl. Phys. Lett.* **87**, 013109 (2005).
- <sup>14</sup>H. Amekura and N. Kishimoto, in *Lecture Notes in Nanoscale Science and Technology*, edited by Z. Wang (Springer, New York, 2009), Vol. 5, pp. 1–75.
- <sup>15</sup>H. Amekura, M. Tanaka, Y. Katsuya, H. Yoshikawa, H. Shinotsuka, S. Tanuma, M. Ohnuma, Y. Matsushita, K. Kobayashi, C. Buchal, S. Mantl, and N. Kishimoto, *Appl. Phys. Lett.* **96**, 023110 (2010).
- <sup>16</sup>H. Amekura, M. Ohnuma, N. Kishimoto, C. Buchal, and S. Mantl, *J. Appl. Phys.* **104**, 114309 (2008).
- <sup>17</sup>H. Amekura, N. Umeda, Y. Takeda, J. Lu, K. Kono, and N. Kishimoto, *Nucl. Instrum. Methods Phys. Res. B* **230**, 193 (2005).
- <sup>18</sup>T. Ikeda, A. Nisawa, M. Okui, N. Yagi, H. Yoshikawa, and S. Fukushima, *J. Synchrotron Radiat.* **10**, 424 (2003).
- <sup>19</sup>*Tables of Physical Constants*, New ed., edited by S. Iida, K. Ohno, H. Kanzaki, H. Kumagai, and S. Sawada (Asakura, Tokyo, 1978), in Japanese.
- <sup>20</sup>U. Kreibitz and M. Vollmer, *Optical Properties of Metal Clusters* (Springer-Verlag, Berlin, Heidelberg, New York, 1995).
- <sup>21</sup>P. A. Stolk, F. W. Saris, A. J. M. Bernsten, W. F. van der Weg, L. T. Sealy, R. C. Barklie, G. Krotz, and G. Muller, *J. Appl. Phys.* **75**, 7266 (1994).
- <sup>22</sup>S. Kondo, H. Tanaka, and T. Saito, *Solid State Commun.* **112**, 665 (1999).
- <sup>23</sup>As mentioned in the text, we used a conventional double-beam spectrometer with a HT chamber installed in the sample space. The sample was illuminated by monochromatic light from a grating, and the transmitted light traveled directly to the detector. In this configuration, thermal radiation from the sample at HT also directly traveled to the detector without

monochromization. Since the signal was detected by the phase-sensitive technique, the first-order influence of the thermal radiation was excluded. However, the gain of the photomultiplier was automatically determined so as to keep the dc component of the photomultiplier signal constant. With increasing thermal radiation, the gain decreases in this configuration but the transmittance value is still reliable because the transmittance was de-

termined from the intensity ratio of the sample and reference paths. Only the S/N ratio is degraded. Two light sources were used: a halogen lamp (0.73–3.65 eV) and a deuterium (D<sub>2</sub>) lamp (3.65–5.90 eV). Since the maximum intensity of the D<sub>2</sub> lamp in the UV region was approximately two orders lower than that of the halogen lamp in the visible region, a very noisy signal was observed only in the UV region.